doi:10.1016/j.jmb.2012.04.009 J. Mol. Biol. (2012) 420, 99–111

Contents lists available at www.sciencedirect.com

Journal of Molecular Biology

journal homepage: http://ees.elsevier.com.jmb

Structural Comparison of Mouse and Human α-Synuclein Amyloid Fibrils by Solid-State NMR

Guohua Lv[1], Ashutosh Kumar[1], Karin Giller[1], Maria L. Orcellet[2], Dietmar Riedel[3], Claudio O. Fernández[2], Stefan Becker[1] and Adam Lange[1]*

[1]*Department of NMR-Based Structural Biology, Max Planck Institute for Biophysical Chemistry, Am Fassberg 11, 37077 Goettingen, Germany*
[2]*Instituto de Biología Molecular y Celular de Rosario, Consejo Nacional de Investigaciones Científicas y Técnicas, Universidad Nacional de Rosario, Suipacha 531, S2002LRK Rosario, Argentina*
[3]*Laboratory for Electron Microscopy, Max Planck Institute for Biophysical Chemistry, Am Fassberg 11, 37077 Goettingen, Germany*

Received 20 January 2012; received in revised form 19 March 2012; accepted 4 April 2012
Available online 16 April 2012

Edited by R. W. Kriwacki

Keywords:
Parkinson's disease;
magic-angle spinning;
sequential assignment strategy;
secondary structure;
supramolecular arrangement

Fibrillar α-synuclein (AS) is the major component of Lewy bodies, the pathological hallmark of Parkinson's disease. Mouse AS (mAS) aggregates much faster than human AS (hAS), although mAS differs from hAS at only seven positions in its primary sequence. Currently, little is known about the site-specific structural differences between mAS and hAS fibrils. Here, we applied state-of-the-art solid-state nuclear magnetic resonance (ssNMR) methods to structurally characterize mAS fibrils. The assignment strategy employed a set of high-resolution 2D and 3D ssNMR spectra recorded on uniformly [^{13}C, ^{15}N], [1-^{13}C]glucose, and [2-^{13}C]glucose labeled mAS fibrils. An almost complete resonance assignment (96% of backbone amide ^{15}N and 93% of all ^{13}C nuclei) was obtained for residues from Gly41 to Val95, which form the core of mAS fibrils. Six β-strands were identified to be within the fibril core of mAS based on a secondary chemical shift and NHHC analysis. Intermolecular ^{13}C:^{15}N labeled restraints obtained from mixed 1:1 ^{13}C/^{15}N-labeled mAS fibrils reveal a parallel, in-register supramolecular β-sheet arrangement. The results were compared in detail to recent structural studies on hAS fibrils and indicate the presence of a structurally conserved motif comprising residues Glu61–Lys80.

Introduction

Parkinson's disease (PD) is a neurodegenerative pathology characterized by the loss of dopaminergic neurons in the substantia nigra region of the brain and the formation of Lewy bodies (LBs)[1] whose major component is α-synuclein (AS)[2–4] in the form of amyloid fibrils. The aggregation of the 140-residue-long cytoplasmic protein AS is thus believed to play an important role in the etiology of PD. AS has been classified as a "natively unfolded" or disordered monomeric protein, which can adopt α-helical structure in solutions that contain lipid-mimetic detergent micelles or in the presence of lipid vesicles.[5–7] The primary sequence of mouse AS (mAS) differs from human AS (hAS) at seven positions (Fig. 1b).[8] An *in vitro* study showed that mAS has a "natively unfolded" structure in solution

*Corresponding author. E-mail address: adla@nmr.mpibpc.mpg.de.

Abbreviations used: AS, α-synuclein; LB, Lewy body; PD, Parkinson's disease; mAS, mouse AS; hAS, human AS; ssNMR, solid-state nuclear magnetic resonance; EM, electron microscopy; 2D, two-dimensional.

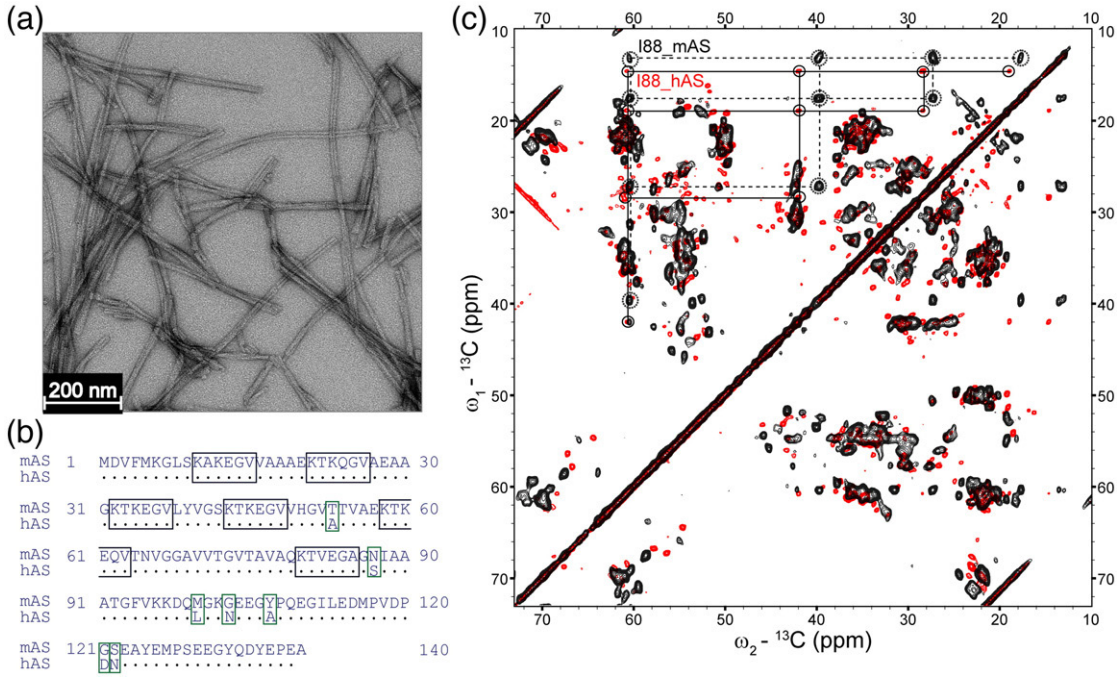

Fig. 1. Initial comparison of mAS and hAS fibrils. (a) Electron micrograph of [U-^{13}C/^{15}N]-labeledmAS fibrils used for ssNMR experiments. (b) Primary sequence alignment of mAS and hAS. The seven mutation sites are indicated with green boxes. The six highly repetitive, imperfect KTKEGV motifs are shown in black boxes. (c) Comparison of 2D PDSD spectra of [U-^{13}C/^{15}N]-labeled hAS fibrils (black) and [U-^{13}C/^{15}N]-labeled mAS fibrils (red, reproduced from Ref. [46]). Correlations of residue Ile88 for mAS and hAS are illustrated with broken and continuous lines, respectively. mAS and hAS fibrils were obtained under identical fibrillization conditions.

similar to hAS, whereas at elevated concentrations, mAS forms amyloid fibrils with predominant β-sheet secondary structure much more rapidly than its human counterpart.[9] Currently, this enhanced fibrillization is not well understood. Recently, an *in vivo* study indicated that endogenous hAS occurs physiologically as a folded tetramer with predominant helical secondary structure even without the addition of lipid vesicles.[10] Although there could be a big difference of the soluble form between *in vitro* and *in vivo* studies, *in vitro* fibrils have been shown to possess a morphology that closely resembles the one found in LBs of patients with PD.[11–13] Because LBs are a pathological hallmark of PD, extensive research has focused on the structural characterization of AS fibrils.[11–18]

Magic-angle spinning solid-state nuclear magnetic resonance (ssNMR) spectroscopy has emerged as a powerful tool for the characterization of noncrystalline and insoluble proteins,[19] including membrane proteins,[20–25] oligomeric assemblies,[26–31] and amyloid fibrils.[32–39] Extensive studies on hAS fibrils using ssNMR revealed that the central fibril core extends at least from about residue Leu38 to about residue Val95 with mostly β-sheet secondary structure.[14–18] However, much less is known about the structural properties of mAS fibrils. Rochet *et al.* demonstrated the presence of β-sheet secondary structure in mAS fibrils, but the extent of the core region and site-specific structural information remained absent.[9] Meanwhile, one recent study on the detailed sequence-dependent fibrillization differences between mAS and hAS revealed that the Ala53Thr substitution dominates the aggregation growth rates, while the combination of the Ala53Thr and Ser87Asn mutations affects the lag phase of the aggregation.[40] Nevertheless, so far no structural details of mAS fibrils and their differences to hAS fibrils were available which motivated the present study.

Here, we aimed at the structural characterization of mAS fibrils using state-of-the-art ssNMR. As a major bottleneck in structural studies of fibrillar proteins by ssNMR remains the unambiguous and confident sequential resonance assignment that is often difficult due to poorly resolved and highly crowded ssNMR spectra. Furthermore, structural polymorphism can lead to the phenomenon that different sample preparations exhibit slightly different ssNMR spectra. The combination of a highly reproducible sample preparation, tailored isotope labeling schemes, and state-of-the-art ssNMR methods enabled us to obtain the near-complete sequential resonance assignment and a subsequent

structural characterization of the fibril core of mAS fibrils. For this purpose, we prepared uniformly [^{13}C, ^{15}N]-([U-^{13}C/^{15}N]) labeled mAS fibrils, and two complementary sparsely ^{13}C-enriched variants of mAS fibrils. Bacterial growth in media containing [1-^{13}C]glucose ([1-^{13}C]Glc) or [2-^{13}C]glucose ([2-^{13}C]Glc) results in highly diluted ^{13}C labeling in the proteins with only one out of six carbons labeled.[41–43] This leads to enhanced resolution and a reduced number of cross-peaks that facilitates the sequential resonance assignment considerably.[42] Highly confident assignment of 96% of backbone amide ^{15}N and 93% of all ^{13}C atoms of the detected residues from Gly41 to Val95 was obtained. Six β-strands were identified to be within the fibril core of mAS fibrils by secondary chemical shift and NHHC[44] analysis. Additionally, by measurement of intermolecular ^{1}H/^{1}H correlations using the NHHC scheme on a mixed 1:1 ^{13}C:^{15}N ([M-^{13}C/^{15}N]) variant[45] of mAS fibrils, we could deduce the supramolecular arrangement of mAS fibrils. We found that they are stacked parallel and in-register. This result is in agreement with our recent investigation of hAS fibrils prepared under identical fibrillization conditions to the mAS fibrils studied here and that were also found to adopt a parallel, in-register β-sheet arrangement.[46]

Results and Discussion

Morphological characterization by EM and initial comparison to hAS fibrils

In this study, [U-^{13}C/^{15}N]-, [1-^{13}C]Glc-, and [2-^{13}C]Glc-labeled mAS fibrils were prepared under identical conditions to obtain the sequential resonance assignment. The morphology of the three samples was then monitored by electron microscopy (EM). The mAS fibrils were all well ordered, and long straight fibrils with a diameter around 160 Å dominate all three samples (as an example, an EM micrograph of [U-^{13}C/^{15}N]-labeled mAS fibrils is shown in Fig. 1a). Rarely, twisted fibrils were observed in [U-^{13}C/^{15}N]-labeled mAS fibrils, and no twisted fibrils were observed in [1-^{13}C]Glc- or [2-^{13}C]Glc-labeled mAS fibrils. The highly similar morphology of the three samples indicates high reproducibility of our sample preparation, which is an essential requirement if different labeling schemes are to be used for ssNMR. However, both straight and helically twisted fibrils of mAS were observed by EM in the recent study by Kang *et al.*[40] The observed differences of the mAS fibril morphology might be due to different fibrillization conditions and suggests the existence of two types of mAS fibrils (straight and twisted). In the case of hAS fibrils, the overall morphology was demonstrated to be strongly dependent on the fibrillization conditions, and both straight and twisted fibrils were observed and characterized.[14] Nevertheless, the highly uniform morphology of mAS fibrils obtained by our preparation indicates high molecular homogeneity of our samples, and indeed, no detectable polymorphism was observed in our recorded ssNMR spectra (see below). The absence of polymorphism allowed us to obtain sequential resonance assignments of the core region of mAS fibrils with straight morphology.

The primary sequence of mAS differs from hAS at seven positions (Fig. 1b).[8] Despite the highly conserved sequence, the aggregation kinetics of mAS and hAS are remarkably different.[9,40] mAS aggregates about twice faster, and the lag phase is reduced by almost 1 order of magnitude.[40] To characterize the structural differences between mAS and hAS fibrils at the atomic level, we recorded a set of high-resolution ssNMR spectra on mAS fibrils and compared it to existing data for hAS fibrils that were prepared under identical conditions.[46] As an example, Fig. 1c shows the comparison of two-dimensional (2D) PDSD (*p*roton-*d*riven *s*pin *d*iffusion) spectra with a mixing time of 20 ms recorded on hAS (red) and mAS (black) fibrils. The hAS fibrils considered here exhibit the same morphology as mAS fibrils (i.e., straight). From the spectral comparison, a difference between mAS fibrils and hAS fibrils is obvious, as illustrated with the straightforward Ile88 assignment in Fig. 1c. Since the amino acid sequence of mAS differs from hAS at position 87 (Ser *versus* Asn) (Fig. 1b), different chemical shifts of Ile88 due to the disturbance of the chemical environment by the Ser87Asn mutation are expected. A more detailed comparison between mAS and hAS fibrils requires the sequential resonance assignment of mAS fibrils as described in the following section.

Sequential resonance assignment using high-resolution ssNMR spectra

The sequential resonance assignment strategy using 2D ^{13}C/^{15}N and ^{13}C/^{13}C correlation spectra recorded on [U-^{13}C/^{15}N]-labeled mAS fibrils is illustrated in Fig. 2. The recorded NCACX, NCOCX, and 2D PDSD spectra with mixing times of 20 ms and 150 ms were well resolved, and the ^{13}C and ^{15}N linewidths were found to be ~0.5 ppm and ~1.3 ppm, respectively. As an example, the sequential resonance assignment of Gly41–Ser42–Lys43 is illustrated in Fig. 2. Additionally, three-dimensional NCACX and NCOCX spectra were recorded to confirm and obtain more unambiguous assignments (Fig. S1). Taken together, the combination of 2D and three-dimensional ^{13}C/^{15}N and ^{13}C/^{13}C spectra of [U-^{13}C/^{15}N]-labeled mAS fibrils enabled us to obtain the sequential connections for the following stretches unambiguously:

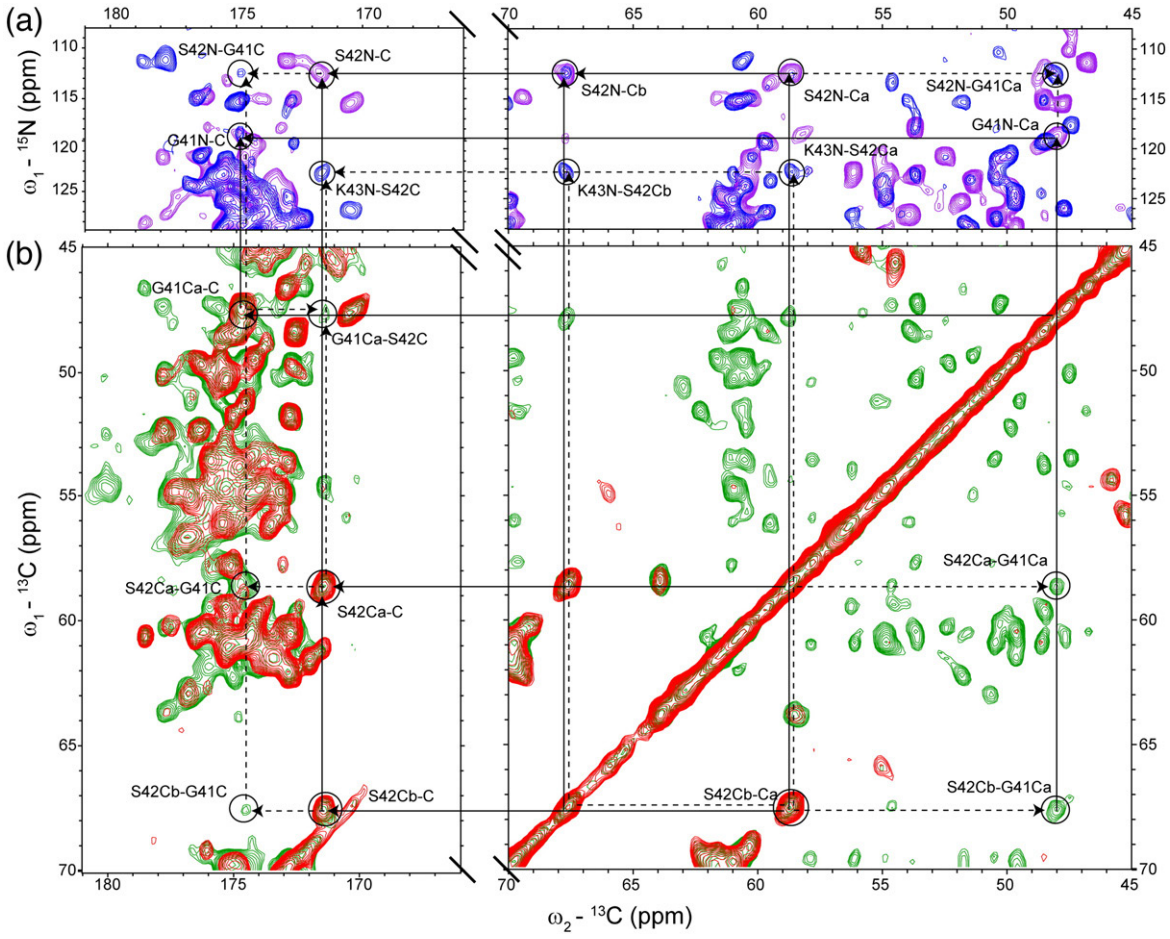

Fig. 2. Sequential resonance assignment strategy using 2D $^{15}N/^{13}C$ and $^{13}C/^{13}C$ correlation spectra recorded on [U-$^{13}C/^{15}N$]-labeled mAS fibrils. Excerpts of carbonyl (left) and aliphatic (right) regions of (a) NCACX (purple) and NCOCX (blue) spectra and (b) 2D PDSD spectra with mixing times of 20 ms (red) and 150 ms (green). Intra- and inter-residue connectivities are illustrated with continuous and broken arrows, respectively.

Gly41–Val48, Ala56–Lys60, Asn65–Val70, and Thr72–Phe94.

The limited resolution and spectral overlap observed for the [U-$^{13}C/^{15}N$]-labeled sample are major obstacles obtaining the complete sequential resonance assignment. Furthermore, the full sequential resonance assignment for mAS fibrils is complicated not only due to the highly repetitive, imperfect KTKEGV motifs (Fig. 1b) but also due to the similar secondary structure adopted by most residues in the β-sheet arrangement. Another difficulty to complete the full assignment of mAS fibrils relates to the high abundance and sequential clustering of Val and Thr, for example, Val48–Val49, Val52–Thr53–Thr54–Val55, Val70–Val71–Thr72, Val74–Thr75, and Thr81–Val82, since the C^{α} and C^{γ} chemical shifts of Val and Thr are similar. In order to alleviate spectral overlap and enhance the resolution, we used sparse ^{13}C labeling schemes. In the sample of [2-^{13}C]Glc-labeled[42,43] mAS fibrils, $^{13}C^{\alpha}$ is labeled for 17 out of 20 residues without simultaneous ^{13}C labeling at C^{β}. With this labeling scheme, not only the resolution is enhanced substantially due to the removal of one-bond ^{13}C-^{13}C J and dipolar couplings but also the sequential transfer of $^{13}C^{\alpha}(i)$-$^{13}C^{\alpha}(i\pm1)$ is facilitated by the ^{13}C spin dilution.

Figure 3 illustrates the sequential backbone resonance assignment strategy based on 2D $^{13}C/^{13}C$ and $^{13}C/^{15}N$ correlation spectra recorded on [2-^{13}C]Glc-labeled mAS fibrils. The observed linewidths for ^{13}C and ^{15}N are ~0.3 ppm and ~0.5 ppm, respectively. The aliphatic and carbonyl regions of a 2D PDSD spectrum with long mixing time of 500 ms are dominated by $^{13}C^{\alpha}(i)$-$^{13}C^{\alpha}(i\pm1)$ and $^{13}C^{\alpha}(i)$-^{13}CO $(i-1)$ correlations, respectively (Fig. 3a). Sequential assignments involve $^{13}C^{\alpha}(i)$-$^{13}C^{\alpha}(i\pm1)$ correlations, which can be easily connected to $^{15}N(i)$-$^{13}C^{\alpha}(i)$ correlations in the NCA spectrum (Fig. 3c). Then the $^{13}CO(i-1)$ resonances can be identified via the

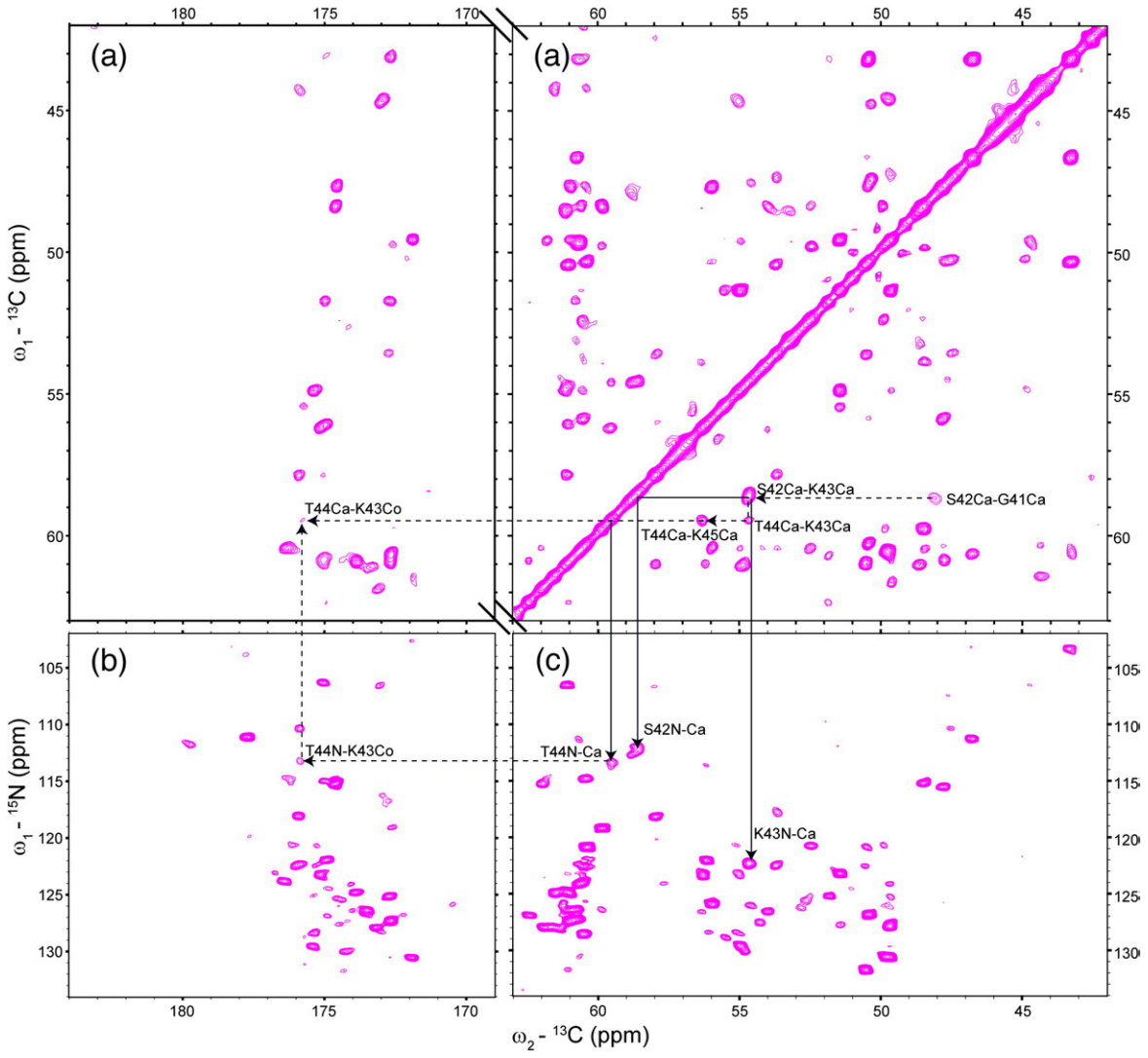

Fig. 3. Sequential assignment strategy for backbone resonances using [2-^{13}C]Glc-labeled mAS fibrils. (a) Carbonyl and aliphatic regions of a PDSD spectrum recorded with a mixing time of 500 ms; (b) NCO and (c) NCA spectra. The sequential backbone assignment of Gly41–Thr44 is shown to exemplify the assignment strategy. Intra- and inter-residue connectivities are indicated with continuous and broken arrows, respectively.

$^{13}C^{\alpha}(i)$ resonances in the carbonyl region of the 2D PDSD spectrum (Fig. 3a) and/or from the $^{15}N(i)$ resonances in the NCO spectrum (Fig. 3b). As an example, the broken arrows show the sequential connections from Gly41 to Thr44, and the continuous arrows show the intra-residue connections for residues Ser42 to Thr44 (Fig. 3). It is worth to note that $^{13}C^{\alpha}$ and $^{13}C^{\beta}$ are labeled simultaneously for Val using this labeling scheme, which enabled us to obtain and confirm the assignments of Val by sequential $^{13}C^{\beta}(i)$-$^{13}C^{\alpha}(i\pm1)$ correlations (Fig. 4). Also, the presence of $^{15}N(i)$-$^{13}C^{\beta}(i)$ correlations for Val in the NCA spectrum due to the attenuation of dipolar truncation effects[47] by the sparse ^{13}C labeling scheme allowed for the unambiguous assignments of $^{15}N(i)$-$^{13}C^{\alpha}(i)$ correlations of Val, although they heavily overlap with the ones of Thr (Fig. S2). In summary, the sequential walks involving $^{13}C^{\alpha}(i)$-$^{13}C^{\alpha}(i\pm1)$ correlations and/or $^{13}C^{\beta}(i)$-$^{13}C^{\alpha}(i\pm1)$ (for Val) correlations lead to sequential resonance assignments for the stretches Gly41–Val49, Gly51–Val52, Thr54–Lys60, Gln62–Val70, Thr72–Val74, and Thr75–Val95 without ambiguity (Fig. 4). In addition, doubling of resonances for the residues Gly84, Ala85, Gly86, Ala89, Gly93, and Phe94 was revealed by the sufficient resolution resulting from the sparse glucose labeling scheme (Fig. 4). A single set of resonances is observed for the other residues, indicating that no polymorphism exists in our samples, whereas the presence of the few doubled resonances may suggest local disorder of these

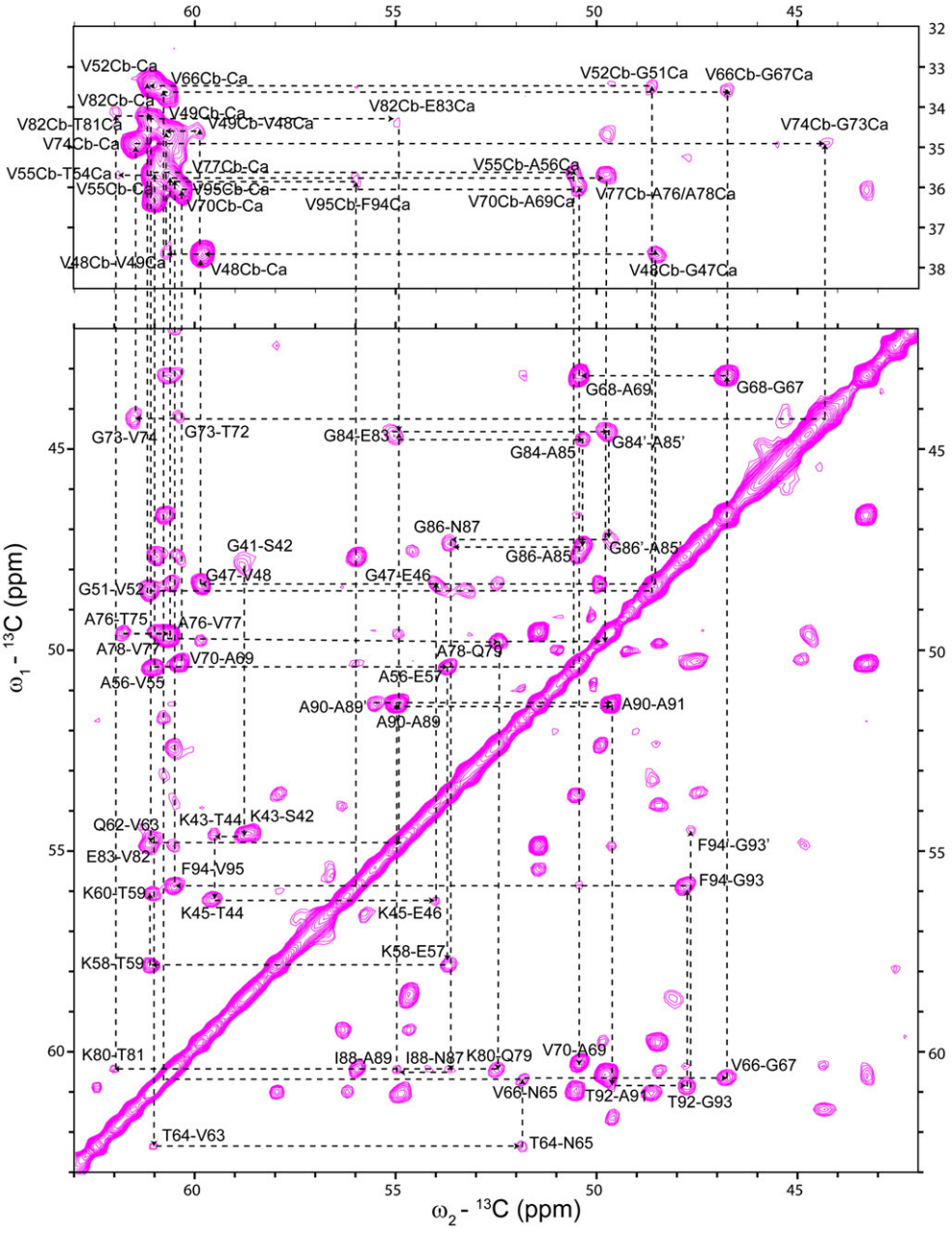

Fig. 4. Sequential walks in a 2D PDSD spectrum recorded with a mixing time of 500 ms of [2-^{13}C]Glc-labeled mAS fibrils. The sequential walks involve $^{13}C^{\alpha}(i)$-$^{13}C^{\alpha}(i\pm1)$ correlations (lower plot) and Val $^{13}C^{\beta}(i)$-$^{13}C^{\alpha}(i\pm1)$ correlations (upper plot) for the stretches Gly41–Val49, Gly51–Val52, Thr54–Lys60, Gln62–Val70, Thr72–Val74, and Thr75–Val95. The second set of sequential resonance assignments observed is indicated with primes, for example, Phe94′.

residues. This correlates quite well with their location in the secondary structure of mAS fibrils: Gly84 and Ala85 are close to one loop that includes Gly86 and Ala89, while Gly93 and Phe94 are located at the end of the structured region of mAS fibrils (see the discussion about the secondary structure analysis below).

As a perfectly complementary labeling scheme, [1-^{13}C]Glc-labeled[41,42] mAS fibrils were prepared to identify and/or confirm both backbone and side-chain assignments of Thr, Asn, Asp, Gln, Glu, Lys, and Ile. Figure S3 shows the assignment of Thr and Val based on the combination of a PDSD spectrum with a mixing time of 700 ms recorded on [2-^{13}C]Glc-labeled mAS fibrils and PDSD (mixing time: 400 ms), NCO, and NCA spectra recorded on [1-^{13}C]Glc-labeled mAS fibrils. Broken lines in Fig. S3 illustrate the unambiguous

assignment of the critical residue Thr53, one of the two variant sites between hAS and mAS located in the fibril core.

Taken together, the near-complete sequential resonance assignment for residues from Gly41 to Val95 is obtained with all the recorded spectra. In total, 96% of backbone amide ^{15}N and 93% of all ^{13}C resonances (97% of the backbone and 89% of the side chains) are obtained for the detected residues from Gly41 to Val95 (Table S1). To the best of our knowledge, our study reports the sequential resonance assignments of mAS fibrils for the first time and with more complete information compared to hAS fibrils.

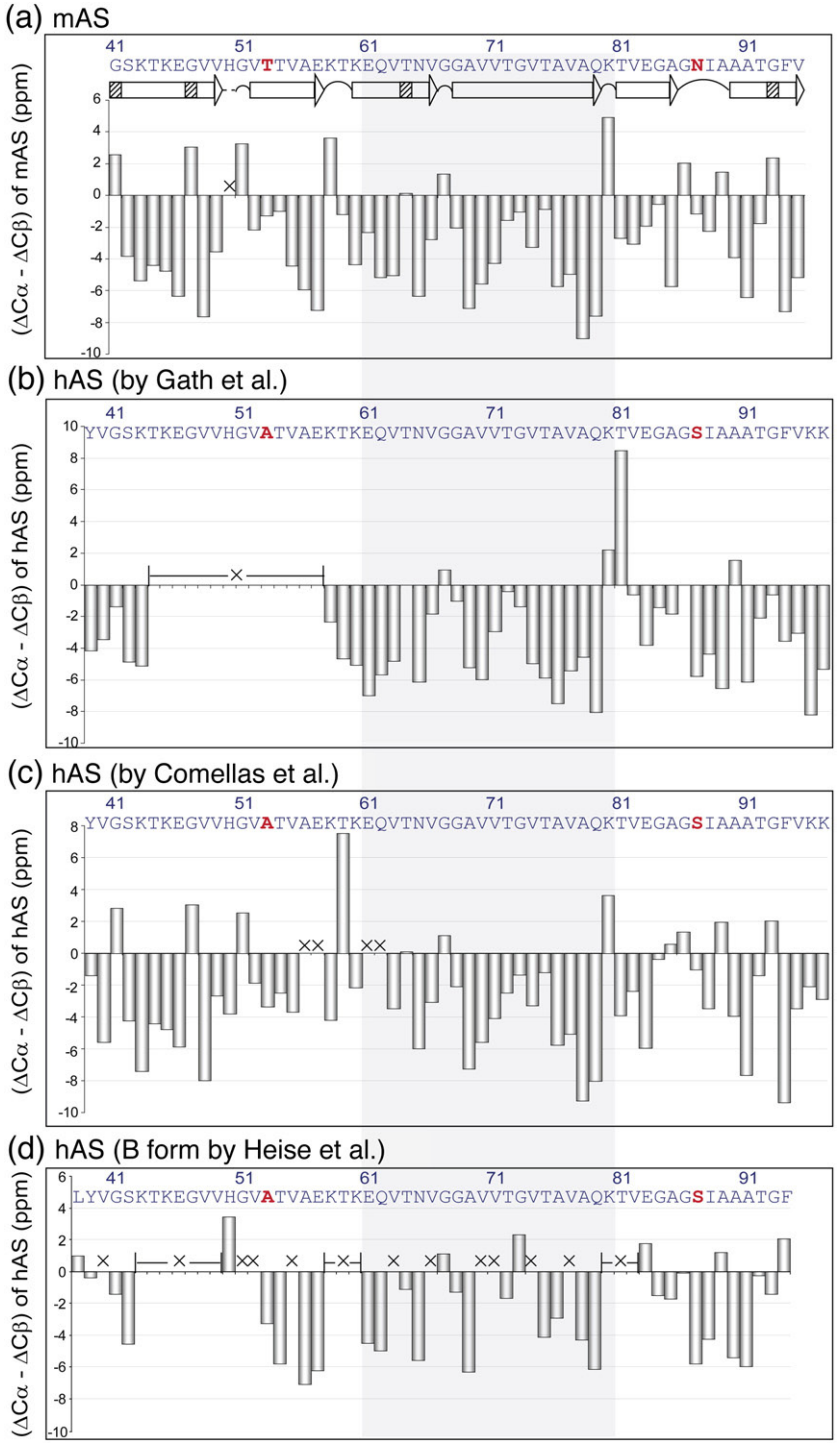

Fig. 5. Secondary structure analysis of the rigid core of mAS fibrils and the comparison to hAS fibrils. Secondary chemical shifts ($\Delta C^{\alpha} - \Delta C^{\beta}$) are shown as a function of residue for (a) mAS fibrils as studied here and hAS fibrils as investigated by (b) Gath *et al.*[18] (for the sake of clarity, the values for residues Met1–Leu38 are omitted), (c) Comellas *et al.*,[17] and (d) Heise *et al.*[14] (B-Form hAS fibrils with straight morphology). For hAS fibrils, no $^{13}C^{\beta}$ assignment was available for Val66 and Phe94 [in (b)] and for His50, Lys60, Lys96, and Lys97 [in (c)]. Non-assigned residues are marked with a cross. The secondary structure of the rigid core of mAS fibrils is illustrated in (a). β-Strands are indicated by white arrows (slashed bars in the white arrow represent possible kinks), non-β-strand regions (kink, loop, or turn) are shown as a curve, and non-assigned amino acids are shown as a broken line. The Ala53Thr and Ser87-Asn variant sites in the rigid core are colored red. The conserved region of AS fibrils as revealed by the comparison of mAS and hAS fibrils studied by Gath *et al.*[18] and Comellas *et al.*[17] is highlighted in gray.

Secondary structure analysis of the fibril core of mAS fibrils and detailed comparison to hAS fibrils

The secondary structure of the rigid core of mAS fibrils was analyzed based on secondary chemical shifts $\{\Delta C^{\alpha} - \Delta C^{\beta} = [\Delta C^{\alpha}(obs) - \Delta C^{\alpha}(rc)] - [\Delta C^{\beta}(obs) - \Delta C^{\beta}(rc)]\}$[48] and is illustrated in Fig. 5a. For all the residues apart from Gly, three or more continuous negative values of $(\Delta C^{\alpha} - \Delta C^{\beta})$ are indicative of β-strand conformation, while positive values point to α-helical structure, and values close to 0 indicate a random-coil conformation. As an independent and complementary indicator, backbone $^{1}H/^{1}H$ distances were probed indirectly using the NHHC scheme[44] to characterize the secondary structure of mAS fibrils (Fig. S4). Longitudinal $^{1}H/^{1}H$ mixing times of 150 μs and 175 μs for [U-$^{13}C/^{15}N$]- and [2-^{13}C]Glc-labeled mAS fibrils, respectively, were used. The enhanced resolution of the NHHC spectrum of [2-^{13}C]Glc-labeled mAS fibrils compared to the spectrum of [U-$^{13}C/^{15}N$]-labeled mAS fibrils facilitated the site-specific identification of secondary structure. Observed $^{15}NH(i+1)$-$^{13}C^{\alpha}H(i)$ correlations with stronger intensities compared to $^{15}NH(i)$-$^{13}C^{\alpha}H(i)$ correlations or the exclusive presence of $^{15}NH(i+1)$-$^{13}C^{\alpha}H(i)$ correlations, as seen, for example, for Ser42 and Lys43, are indicative of β-sheet conformation. In contrast, the clear absence of $^{15}NH(i+1)$-$^{13}C^{\alpha}H(i)$ correlations or the presence with weaker intensities compared to $^{15}NH(i)$-$^{13}C^{\alpha}H(i)$ correlations, for example, observed for Lys58 and Thr59, is indicative of loop or turn structure. Together with the secondary chemical shifts, six β-strands were identified to be within the fibril core of mAS fibrils: Gly41–Val49, Val52–Glu57, Lys60–Val66, Gly68–Gln79, Thr81–Ala85, and Ala90–Val95. Possible kinks in the β-strands are marked by slashed bars (Fig. 5a).

A direct comparison between mAS and hAS fibrils has to take into account the existence of multiple sets of chemical shifts, incomplete sequential resonance assignments, and the presence of different morphologies of hAS fibrils. For example, 48 residues (form A, twisted fibrils) and 36 residues (form B, straight fibrils) from Leu38 to Val95 were assigned and identified to be within the fibril core of hAS for two distinct fibril morphologies by Heise *et al.*[14] Recently, sequential resonance assignments for 85% of residues from Met1 to Lys97 were achieved by Gath *et al.*,[18] and 91% of the ^{15}N and ^{13}C resonances of residues from Leu38 to Lys96 were reported by Comellas *et al.*[17] Collectively, hAS fibrils seem to recruit more residues into the β-sheet fibril core than mAS fibrils. Residues from Gly41 to Val95 were sequentially assigned and identified to be within the fibril core of mAS fibrils by our current work. The assignment of Val40 was obtained ambiguously. Unambiguous assignments for residues of Leu38 and Tyr39 could so far not be obtained due to a lack of sequential correlations. This might be because these two residues are at the beginning of the structured region, and the peak intensities may thus be too weak to be observed. On the other hand, there are clearly no detectable sequential connections from Val95 to Lys96 in our spectra. However, we were able to find residues outside the identified fibril core in PDSD spectra, such as Ser (Ser9 or Ser129), Pro (Pro108, Pro117, Pro120, Pro128, or Pro138), and Asp (Asp2, Asp98, Asp115, Asp119, or Asp135). However, we could not detect any sequential connections to assign them unambiguously. Importantly, the Ser and Pro resonances are absent in a DREAM (*d*ipolar *r*ecoupling *e*nhancement through *a*mplitude *m*odulation) spectrum (see Fig. S5), which may indicate that they are relatively flexible. This is corroborated by the observation that the Ser and Pro signals have random-coil chemical shifts, whereas the unassigned Asp exhibits β-strand-like chemical shifts (See Table S1).

The B-Form hAS fibrils studied by Heise *et al.* are straight, while the A-Form has a twisted morphology.[14] However, the fibril morphology was not reported in the publications by Gath *et al.*[18] and Comellas *et al.*[17] on hAS fibrils. Because the ssNMR spectra are virtually identical for hAS fibrils as reported by Gath *et al.*[18] and by us (see Fig. 1, straight fibrils, produced under the same conditions as the mAS fibrils with straight morphology reported in the current study),[46] we assume that Gath *et al.* also obtained straight fibrils. However, no EM micrograph is shown in Gath *et al.*[18] The fibril morphology for Comellas *et al.* is not clear. In the published EM micrograph (Comellas *et al.*,[17] Fig. 8), the fibrils appear straight as well. Interestingly, we see strong differences between mAS and hAS in terms of secondary chemical shifts and extent of β-strand regions if we consider hAS prepared under the same fibrillization conditions as mAS (with assignments for this form reported by Gath *et al.*,[18] see Fig. 5b). The most significant difference relates to residues Met1–Val37 that are only observed in spectra of hAS. In contrast, residues Thr44–Glu57 are only observed for mAS. Furthermore, for several residues in the core, secondary chemical shifts $(\Delta C^{\alpha} - \Delta C^{\beta})$ with opposite sign for mAS and hAS were observed: Gly41, Lys58, Thr81, Ala89, and Ala91. In contrast, much higher similarity was observed between mAS fibrils and hAS fibrils studied by Comellas *et al.* (Fig. 5c),[17] regarding both the length and the location of the β-strands. The only residues that adopt a significantly different secondary structure (i.e., opposite sign of the secondary chemical shift) in mAS and hAS fibrils studied by Comellas *et al.*[17] (Fig. 5c) are Lys58, Thr59, and Ala85. The systematic structural comparison between mAS fibrils and the two different

forms of hAS fibrils reveals that residues Glu61–Lys80 constitute the structurally most conserved region of AS. Interestingly, the mutation sites of Ala53Thr and Ser87Asn that are responsible for the differences in aggregation kinetics and lag phases between mAS and hAS are outside this region. The conserved core of Glu61–Lys80 might play an important role in the initiation of the aggregation of AS fibrils. Consistent with this notion, it was previously reported that residues Glu61–Ala78,[49] Gly68–Ala78,[50] and Val71–Val82[51] within the hydrophobic region of AS could form aggregates by themselves *in vitro* and that residues Gly68–Ala78[50] constitute the shortest fragment sufficient for AS fibril assembly.

Supramolecular structure of mAS fibrils elucidated by means of [M-^{13}C/^{15}N]-labeled mAS fibrils

Previous ssNMR studies on heterogeneously labeled samples have yielded structural insight into the supramolecular arrangement of amyloid fibrils.[33,45,52–58]. Here, we have recorded an NHHC[44] spectrum with a ^{1}H/^{1}H mixing time of 500 μs on [M-^{13}C/^{15}N]-labeled mAS fibrils to elucidate the stacking of molecules in the fibrils. With the chosen mixing time, cross-peaks between ^{13}C and ^{15}N sites that correspond to intermolecular (^{1}H/^{1}H) distances of about 3.5 Å can be observed.[45] Since ^{15}N and ^{13}C spins in the [M-^{13}C/^{15}N]-labeled mAS fibrils are not labeled within the same molecule, all the observed cross-peaks in the NHHC spectrum are exclusively due to intermolecular transfer. As shown in Fig. 6a, most of the cross-peaks can be assigned to either inter-strand ^{15}N(i)-^{13}C$^{\alpha}$(i) or inter-strand ^{15}N(i)-^{13}C$^{\alpha}$($i-1$) correlations. These contacts are summarized in Fig. 6b. The sensitivity of the intermolecular NHHC experiment is compromised due to (a) the three involved CP transfer steps; (b) the probability of one pair of neighboring molecules to be ^{15}N/^{13}C labeled, which is only 25%; (c) the long intermolecular distances involved; and (d) the distribution of magnetization during the ^{1}H/^{1}H transfer to protons that are not involved in the last transfer step. Still, the unambiguous intermolecular correlation pattern, for example, for Lys43, Glu46, and Glu57 (Fig. 6b), as well as the overall good overlay with the NCA spectrum recorded on [U-^{13}C/^{15}N]-labeled mAS fibrils (Fig. 6a), identifies a parallel, in-register arrangement of the β-strands. This result is in agreement with a similar recent study by our group showing that the hAS fibrils studied by us are stacked parallel and in-register.[46]

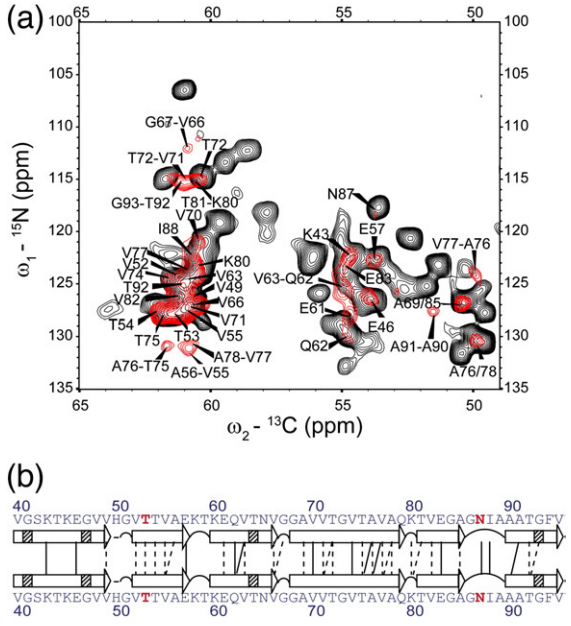

Fig. 6. Supramolecular arrangement of mAS fibrils. (a) Comparison of NCA spectrum (in black) recorded on [U-^{13}C/^{15}N]-labeled mAS fibrils and NHHC spectrum (in red) recorded on [M-^{13}C/^{15}N]-labeled mAS fibrils. ^{15}N(i)-^{13}C$^{\alpha}$(i) correlations and ^{15}N(i)-^{13}C$^{\alpha}$($i-1$) correlations between adjacent molecules were labeled as, for example, Val63 and Val63–Gln62, respectively. (b) Summary of the detected intermolecular contacts. Continuous lines represent unambiguous assignments, and broken lines represent ambiguous assignments due to spectral overlap.

Conclusions

We recently reported a strategy for simplified and complete resonance assignment using the ^{13}C spin dilution approach, demonstrated with the *de novo* assignment of the type three secretion system needle protein PrgI in the polymerized state, in which most residues adopt α-helical conformation.[42] In the present work, as the second example, the substantially improved spectral resolution observed for [1-^{13}C]Glc- and [2-^{13}C]Glc-labeled mAS fibrils turned out to be highly useful for the near-complete sequential assignment of the β-sheet-rich amyloid fibrils formed by mAS.

The structural comparison between mAS fibrils and two different forms of hAS fibrils reveals that residues Glu61–Lys80 constitute the structurally most conserved region of AS. While the Glu61–Lys80 conserved core appears to play a critical role as an initiator of aggregation, a subtle modulatory effect might be exerted on the AS aggregation pathway by mutations located inside the extended fibrillogenic region formed by residues Gly41–Val95. Indeed, it was reported recently that the Ala53Thr substitution dominates the aggregation growth rates, while the combination of the Ala53Thr and Ser87Asn mutations affects the lag phase of the aggregation of mAS compared to hAS.[40]

It should be worthwhile to determine structures of mAS and hAS fibrils in order to gain further insights into the largely different aggregation kinetics. Currently, we are exploiting the improved resolution and reduced dipolar truncation in the sparsely labeled mAS samples, to collect long-range distance restraints with the aim of an atomic model of mAS amyloid fibrils.

Materials and Methods

Sample preparation and morphology characterization

mAS samples labeled with [U-^{13}C/^{15}N], [1-^{13}C]Glc, and [2-^{13}C]Glc were produced using [U-^{13}C]glucose, [1-^{13}C]glucose, and [2-^{13}C]glucose, respectively, as the sole carbon source in the bacterial growth medium. These three samples were uniformly ^{15}N labeled. [M-^{13}C/^{15}N]-labeled mAS fibrils were prepared by aggregating an equimolar mixture of ^{13}C-labeled and ^{15}N-labeled mAS. Fibrillization of mAS was achieved according to the protocol previously developed for hAS.[14] In short, mAS solutions were incubated with protein concentrations of 200 μM in 25 mM Tris–HCl buffer, pH 7.5, containing 0.02% NaN_3 at 37 °C with continuous stirring with micro stir bars at 300 rpm until the concentration of fibrillized protein reached a steady state according to a thioflavin T fluorescence assay.[59] The morphology of the mAS fibrils was monitored by negative-stained EM at room temperature.

ssNMR experiments and analysis

All ssNMR experiments were conducted using 4-mm and 3.2-mm triple-resonance (^{1}H, ^{13}C, ^{15}N) probe heads at static magnetic fields of 20 T, 18.8 T, and 14.1 T, corresponding to 850 MHz, 800 MHz, and 600 MHz ^{1}H resonance frequencies (Bruker BioSpin, Germany). The chemical shifts of ^{13}C and ^{15}N were calibrated either with 2,2-dimethyl-2-silapentane-5-sulfonate as an internal reference[60] or with adamantane as an external reference.[61] Sample temperatures were determined by the position of the water ^{1}H resonance using the relation $\delta(H_2O) = 7.83 - T/96.9$[62] All experiments were carried out at a sample temperature of around +278 K and magic-angle spinning rates between 11 kHz and 18 kHz. An initial ramped cross-polarization[63,64] was used to transfer the magnetization from ^{1}H to ^{13}C or ^{15}N with contact times between 400 μs and 1000 μs, and ^{15}N-to-^{13}C transfer was achieved using SPECIFIC cross-polarization[65] with contact times of 3–6 ms. SPINAL-64 high-power proton decoupling[66] was applied during evolution and detection periods with radiofrequency amplitudes of 69–83 kHz. DREAM[67] spectra employed a recoupling period of 4 ms. Double-quantum single-quantum correlation spectra were recorded with the SPC5 scheme.[68] ^{13}C/^{13}C correlation experiments were conducted using PDSD or DARR (*d*ipolar *a*ssisted *r*otational *r*esonance)[69] with different mixing times. ^{1}H/^{1}H distances were probed indirectly by using the NHHC[44] scheme. All spectra were processed with Topspin and analyzed in SPARKY version 3.1 (T. D. Goddard and D. G. Kneller, University of California).

Accession numbers

Chemical shift assignments have been deposited to the BioMagResBank for release upon publication (BioMagResBank entry number 18232 for mAS fibrils).

Acknowledgements

We are grateful to C. Griesinger for continuous support of our work, B. Angerstein for expert technical assistance, and A. Loquet for the 2D PDSD spectrum of hAS fibrils. We thank the Max Planck Society, the Deutsche Forschungsgemeinschaft (Emmy Noether fellowship to A.L.), the China Scholarship Council (PhD scholarship to G.L.), and the Marie Curie IIF Fellowship within the Seventh European Community Framework Programme (fellowship to A.K.) for financial support. C.O.F. thanks Agencia Nacional de Promoción Científica y Tecnológica, the Max Planck Society, and the Alexander von Humboldt Foundation for financial support. C.O.F. is the head of a Partner Group of the Max Planck Institute for Biophysical Chemistry (Goettingen). M.L.O. is a recipient of a fellowship from Agencia Nacional de Promoción Científica y Tecnológica.

Supplementary Data

Supplementary data associated with this article can be found, in the online version, at doi:10.1016/j.jmb.2012.04.009

References

1. Forno, L. S. (1996). Neuropathology of Parkinson's disease. *J. Neuropathol. Exp. Neurol.* **55**, 259–272.
2. Spillantini, M. G., Schmidt, M. L., Lee, V. M. Y., Trojanowski, J. Q., Jakes, R. & Goedert, M. (1997). α-Synuclein in Lewy bodies. *Nature*, **388**, 839–840.
3. Spillantini, M. G., Crowther, R. A., Jakes, R., Hasegawa, M. & Goedert, M. (1998). α-Synuclein in filamentous inclusions of Lewy bodies from Parkinson's disease and dementia with Lewy bodies. *Proc. Natl Acad. Sci. USA*, **95**, 6469–6473.
4. Baba, M., Nakajo, S., Tu, P. H., Tomita, T., Nakaya, K., Lee, V. M. Y. *et al.* (1998). Aggregation of α-synuclein in Lewy bodies of sporadic Parkinson's disease and dementia with Lewy bodies. *Am. J. Pathol.* **152**, 879–884.
5. Weinreb, P. H., Zhen, W. G., Poon, A. W., Conway, K. A. & Lansbury, P. T. (1996). NACP, a protein implicated in Alzheimer's disease and learning, is natively unfolded. *Biochemistry*, **35**, 13709–13715.
6. Eliezer, D., Kutluay, E., Bussell, R. Jr & Browne, G. (2001). Conformational properties of α-synuclein in its

free and lipid-associated states. *J. Mol. Biol.* **307**, 1061–1073.
7. Davidson, W. S., Jonas, A., Clayton, D. F. & George, J. M. (1998). Stabilization of α-synuclein secondary structure upon binding to synthetic membranes. *J. Biol. Chem.* **273**, 9443–9449.
8. Hong, L., Ko, H. W., Gwag, B. J., Joe, E., Lee, S., Kim, Y. T. & Suh, Y. H. (1998). The cDNA cloning and ontogeny of mouse α-synuclein. *NeuroReport*, **9**, 1239–1243.
9. Rochet, J. C., Conway, K. A. & Lansbury, P. T. (2000). Inhibition of fibrillization and accumulation of prefibrillar oligomers in mixtures of human and mouse α-synuclein. *Biochemistry*, **39**, 10619–10626.
10. Bartels, T., Choi, J. G. & Selkoe, D. J. (2011). α-Synuclein occurs physiologically as a helically folded tetramer that resists aggregation. *Nature*, **477**, 107–110.
11. Conway, K. A., Harper, J. D. & Lansbury, P. T. (2000). Fibrils formed *in vitro* from α-synuclein and two mutant forms linked to Parkinson's disease are typical amyloid. *Biochemistry*, **39**, 2552–2563.
12. Serpell, L. C., Berriman, J., Jakes, R., Goedert, M. & Crowther, R. A. (2000). Fiber diffraction of synthetic α-synuclein filaments shows amyloid-like cross-β conformation. *Proc. Natl Acad. Sci. USA*, **97**, 4897–4902.
13. Miake, H., Mizusawa, H., Iwatsubo, T. & Hasegawa, M. (2002). Biochemical characterization of the core structure of α-synuclein filaments. *J. Biol. Chem.* **277**, 19213–19219.
14. Heise, H., Hoyer, W., Becker, S., Andronesi, O. C., Riedel, D. & Baldus, M. (2005). Molecular-level secondary structure, polymorphism, and dynamics of full-length α-synuclein fibrils studied by solid-state NMR. *Proc. Natl Acad. Sci. USA*, **102**, 15871–15876.
15. Kloepper, K. D., Zhou, D. H., Li, Y., Winter, K. A., George, J. M. & Rienstra, C. M. (2007). Temperature-dependent sensitivity enhancement of solid-state NMR spectra of α-synuclein fibrils. *J. Biomol. NMR*, **39**, 197–211.
16. Vilar, M., Chou, H. T., Luhrs, T., Maji, S. K., Riek-Loher, D., Verel, R. *et al.* (2008). The fold of α-synuclein fibrils. *Proc. Natl Acad. Sci. USA*, **105**, 8637–8642.
17. Comellas, G., Lemkau, L. R., Nieuwkoop, A. J., Kloepper, K. D., Ladror, D. T., Ebisu, R. *et al.* (2011). Structured regions of α-synuclein fibrils include the early-onset Parkinson's disease mutation sites. *J. Mol. Biol.* **411**, 881–895.
18. Gath, J., Habenstein, B., Bousset, L., Melki, R., Meier, B. H. & Bockmann, A. (2011). Solid-state NMR sequential assignments of α-synuclein. *Biomol. NMR Assignments*, **6**, 51–55.
19. Renault, M., Cukkemane, A. & Baldus, M. (2010). Solid-state NMR spectroscopy on complex biomolecules. *Angew. Chem., Int. Ed. Engl.* **49**, 8346–8357.
20. Cady, S. D., Schmidt-Rohr, K., Wang, J., Soto, C. S., Degrado, W. F. & Hong, M. (2010). Structure of the amantadine binding site of influenza M2 proton channels in lipid bilayers. *Nature*, **463**, 689–692.
21. Shi, L., Ahmed, M. A., Zhang, W., Whited, G., Brown, L. S. & Ladizhansky, V. (2009). Three-dimensional solid-state NMR study of a seven-helical integral membrane proton pump—structural insights. *J. Mol. Biol.* **386**, 1078–1093.
22. Schneider, R., Etzkorn, M., Giller, K., Daebel, V., Eisfeld, J., Zweckstetter, M. *et al.* (2010). The native conformation of the human VDAC1 N terminus. *Angew. Chem., Int. Ed. Engl.* **49**, 1882–1885.
23. Lange, A., Giller, K., Hornig, S., Martin-Eauclaire, M. F., Pongs, O., Becker, S. & Baldus, M. (2006). Toxin-induced conformational changes in a potassium channel revealed by solid-state NMR. *Nature*, **440**, 959–962.
24. Yang, J., Aslimovska, L. & Glaubitz, C. (2011). Molecular dynamics of proteorhodopsin in lipid bilayers by solid-state NMR. *J. Am. Chem. Soc.* **133**, 4874–4881.
25. Jacso, T., Franks, W. T., Rose, H., Fink, U., Broecker, J., Keller, S. *et al.* (2011). Characterization of membrane proteins in isolated native cellular membranes by dynamic nuclear polarization solid-state NMR spectroscopy without purification and reconstitution. *Angew. Chem., Int. Ed. Engl.* **51**, 432–435.
26. Chimon, S., Shaibat, M. A., Jones, C. R., Calero, D. C., Aizezi, B. & Ishii, Y. (2007). Evidence of fibril-like β-sheet structures in a neurotoxic amyloid intermediate of Alzheimer's β-amyloid. *Nat. Struct. Mol. Biol.* **14**, 1157–1164.
27. Jehle, S., Rajagopal, P., Bardiaux, B., Markovic, S., Kuhne, R., Stout, J. R. *et al.* (2010). Solid-state NMR and SAXS studies provide a structural basis for the activation of αB-crystallin oligomers. *Nat. Struct. Mol. Biol.* **17**, 1037–1042.
28. Han, Y., Ahn, J., Concel, J., Byeon, I. J., Gronenborn, A. M., Yang, J. & Polenova, T. (2010). Solid-state NMR studies of HIV-1 capsid protein assemblies. *J. Am. Chem. Soc.* **132**, 1976–1987.
29. Chen, B. & Tycko, R. (2010). Structural and dynamical characterization of tubular HIV-1 capsid protein assemblies by solid state nuclear magnetic resonance and electron microscopy. *Protein Sci.* **19**, 716–730.
30. Goldbourt, A., Day, L. A. & McDermott, A. E. (2010). Intersubunit hydrophobic interactions in Pf1 filamentous phage. *J. Biol. Chem.* **285**, 37051–37059.
31. Morag, O., Abramov, G. & Goldbourt, A. (2011). Similarities and differences within members of the Ff family of filamentous bacteriophage viruses. *J. Phys. Chem. B*, **115**, 15370–15379.
32. Jaroniec, C. P., MacPhee, C. E., Bajaj, V. S., McMahon, M. T., Dobson, C. M. & Griffin, R. G. (2004). High-resolution molecular structure of a peptide in an amyloid fibril determined by magic angle spinning NMR spectroscopy. *Proc. Natl Acad. Sci. USA*, **101**, 711–716.
33. Wasmer, C., Lange, A., Van Melckebeke, H., Siemer, A. B., Riek, R. & Meier, B. H. (2008). Amyloid fibrils of the HET-s(218–289) prion form a β solenoid with a triangular hydrophobic core. *Science*, **319**, 1523–1526.
34. Helmus, J. J., Surewicz, K., Nadaud, P. S., Surewicz, W. K. & Jaroniec, C. P. (2008). Molecular conformation and dynamics of the Y145Stop variant of human prion protein in amyloid fibrils. *Proc. Natl Acad. Sci. USA*, **105**, 6284–6289.
35. Bertini, I., Gonnelli, L., Luchinat, C., Mao, J. & Nesi, A. (2011). A new structural model of Aβ40 fibrils. *J. Am. Chem. Soc.* **133**, 16013–16022.
36. Petkova, A. T., Yau, W. M. & Tycko, R. (2006). Experimental constraints on quaternary structure in

Alzheimer's β-amyloid fibrils. *Biochemistry*, **45**, 498–512.
37. Nielsen, J. T., Bjerring, M., Jeppesen, M. D., Pedersen, R. O., Pedersen, J. M., Hein, K. L. *et al.* (2009). Unique identification of supramolecular structures in amyloid fibrils by solid-state NMR spectroscopy. *Angew. Chem., Int. Ed. Engl.* **48**, 2118–2121.
38. Loquet, A., Bousset, L., Gardiennet, C., Sourigues, Y., Wasmer, C., Habenstein, B. *et al.* (2009). Prion fibrils of Ure2p assembled under physiological conditions contain highly ordered, natively folded modules. *J. Mol. Biol.* **394**, 108–118.
39. Helmus, J. J., Surewicz, K., Surewicz, W. K. & Jaroniec, C. P. (2010). Conformational flexibility of Y145Stop human prion protein amyloid fibrils probed by solid-state nuclear magnetic resonance spectroscopy. *J. Am. Chem. Soc.* **132**, 2393–2403.
40. Kang, L., Wu, K. P., Vendruscolo, M. & Baum, J. (2011). The A53T mutation is key in defining the differences in the aggregation kinetics of human and mouse α-synuclein. *J. Am. Chem. Soc.* **133**, 13465–13470.
41. Hong, M. (1999). Determination of multiple ϕ-torsion angles in proteins by selective and extensive ^{13}C labeling and two-dimensional solid-state NMR. *J. Magn. Reson.* **139**, 389–401.
42. Loquet, A., Lv, G., Giller, K., Becker, S. & Lange, A. (2011). ^{13}C spin dilution for simplified and complete solid-state NMR resonance assignment of insoluble biological assemblies. *J. Am. Chem. Soc.* **133**, 4722–4725.
43. Lundstrom, P., Teilum, K., Carstensen, T., Bezsonova, I., Wiesner, S., Hansen, D. F. *et al.* (2007). Fractional ^{13}C enrichment of isolated carbons using [1-^{13}C]- or [2-^{13}C]-glucose facilitates the accurate measurement of dynamics at backbone C^{α} and side-chain methyl positions in proteins. *J. Biomol. NMR*, **38**, 199–212.
44. Lange, A., Luca, S. & Baldus, M. (2002). Structural constraints from proton-mediated rare-spin correlation spectroscopy in rotating solids. *J. Am. Chem. Soc.* **124**, 9704–9705.
45. Etzkorn, M., Bockmann, A., Lange, A. & Baldus, M. (2004). Probing molecular interfaces using 2D magic-angle-spinning NMR on protein mixtures with different uniform labeling. *J. Am. Chem. Soc.* **126**, 14746–14751.
46. Loquet, A., Giller, K., Becker, S. & Lange, A. (2010). Supramolecular interactions probed by ^{13}C–^{13}C solid-state NMR spectroscopy. *J. Am. Chem. Soc.* **132**, 15164–15166.
47. Hodgkinson, P. & Emsley, L. (1999). The accuracy of distance measurements in solid-state NMR. *J. Magn. Reson.* **139**, 46–59.
48. Luca, S., Filippov, D. V., van Boom, J. H., Oschkinat, H., de Groot, H. J. & Baldus, M. (2001). Secondary chemical shifts in immobilized peptides and proteins: a qualitative basis for structure refinement under magic angle spinning. *J. Biomol. NMR*, **20**, 325–331.
49. El-Agnaf, O. M., Jakes, R., Curran, M. D., Middleton, D., Ingenito, R., Bianchi, E. *et al.* (1998). Aggregates from mutant and wild-type α-synuclein proteins and NAC peptide induce apoptotic cell death in human neuroblastoma cells by formation of β-sheet and amyloid-like filaments. *FEBS Lett.* **440**, 71–75.
50. El-Agnaf, O. M. & Irvine, G. B. (2002). Aggregation and neurotoxicity of α-synuclein and related peptides. *Biochem. Soc. Trans.* **30**, 559–565.
51. Giasson, B. I., Murray, I. V., Trojanowski, J. Q. & Lee, V. M. (2001). A hydrophobic stretch of 12 amino acid residues in the middle of α-synuclein is essential for filament assembly. *J. Biol. Chem.* **276**, 2380–2386.
52. Shewmaker, F., Kryndushkin, D., Chen, B., Tycko, R. & Wickner, R. B. (2009). Two prion variants of Sup35p have in-register parallel β-sheet structures, independent of hydration. *Biochemistry*, **48**, 5074–5082.
53. Bayro, M. J., Debelouchina, G. T., Eddy, M. T., Birkett, N. R., MacPhee, C. E., Rosay, M. *et al.* (2011). Intermolecular structure determination of amyloid fibrils with magic-angle spinning and dynamic nuclear polarization NMR. *J. Am. Chem. Soc.* **133**, 13967–13974.
54. Debelouchina, G. T., Platt, G. W., Bayro, M. J., Radford, S. E. & Griffin, R. G. (2010). Intermolecular alignment in β_2-microglobulin amyloid fibrils. *J. Am. Chem. Soc.* **132**, 17077–17079.
55. Helmus, J. J., Surewicz, K., Apostol, M. I., Surewicz, W. K. & Jaroniec, C. P. (2011). Intermolecular alignment in Y145Stop human prion protein amyloid fibrils probed by solid-state NMR spectroscopy. *J. Am. Chem. Soc.* **133**, 13934–13937.
56. Yang, J., Tasayco, M. L. & Polenova, T. (2008). Magic angle spinning NMR experiments for structural studies of differentially enriched protein interfaces and protein assemblies. *J. Am. Chem. Soc.* **130**, 5798–5807.
57. Nieuwkoop, A. J. & Rienstra, C. M. (2010). Supramolecular protein structure determination by site-specific long-range intermolecular solid state NMR spectroscopy. *J. Am. Chem. Soc.* **132**, 7570–7571.
58. Wickner, R. B., Dyda, F. & Tycko, R. (2008). Amyloid of Rnq1p, the basis of the [*PIN*$^{+}$] prion, has a parallel in-register β-sheet structure. *Proc. Natl Acad. Sci. USA*, **105**, 2403–2408.
59. Hoyer, W., Cherny, D., Subramaniam, V. & Jovin, T. M. (2004). Impact of the acidic C-terminal region comprising amino acids 109–140 on α-synuclein aggregation *in vitro*. *Biochemistry*, **43**, 16233–16242.
60. Markley, J. L., Bax, A., Arata, Y., Hilbers, C. W., Kaptein, R., Sykes, B. D. *et al.* (1998). Recommendations for the presentation of NMR structures of proteins and nucleic acids. IUPAC-IUBMB-IUPAB inter-union task group on the standardization of data bases of protein and nucleic acid structures determined by NMR spectroscopy. *Eur. J. Biochem.* **256**, 1–15.
61. Morcombe, C. R. & Zilm, K. W. (2003). Chemical shift referencing in MAS solid state NMR. *J. Magn. Reson.* **162**, 479–486.
62. Cavanagh, J., Fairbrother, W. J., Palmer, A. G., III, Rance, M. & Skelton, N. J. (2007). *Protein NMR Spectroscopy: Principles and Practice*, 2nd edit. Elsevier Academic Press, New York, NY.
63. Metz, G., Wu, X. L. & Smith, S. O. (1994). Ramped-amplitude cross polarization in magic-angle-spinning NMR. *J. Magn. Reson., Ser. A*, **110**, 219–227.
64. Hediger, S., Meier, B. H. & Ernst, R. R. (1995). Adiabatic passage Hartmann–Hahn cross polarization in NMR under magic angle sample spinning. *Chem. Phys. Lett.* **240**, 449–456.

65. Baldus, M., Petkova, A. T., Herzfeld, J. & Griffin, R. G. (1998). Cross polarization in the tilted frame: assignment and spectral simplification in heteronuclear spin systems. *Mol. Phys.* **95**, 1197–1207.
66. Fung, B. M., Khitrin, A. K. & Ermolaev, K. (2000). An improved broadband decoupling sequence for liquid crystals and solids. *J. Magn. Reson.* **142**, 97–101.
67. Verel, R., Baldus, M., Ernst, M. & Meier, B. H. (1998). A homonuclear spin-pair filter for solid-state NMR based on adiabatic-passage techniques. *Chem. Phys. Lett.* **287**, 421–428.
68. Hohwy, M., Rienstra, C. M., Jaroniec, C. P. & Griffin, R. G. (1999). Fivefold symmetric homonuclear dipolar recoupling in rotating solids: application to double quantum spectroscopy. *J. Chem. Phys.* **110**, 7983–7992.
69. Takegoshi, K., Nakamura, S. & Terao, T. (2001). ^{13}C–^{1}H dipolar-assisted rotational resonance in magic-angle spinning NMR. *Chem. Phys. Lett.* **344**, 631–637.